Supplementary Information

Programmable Ion-Protein Networks from Sodium Caseinate: A Sustainable Platform for Soft Functional Materials

Pietro Tordi,[a,b] Verónica Montes-García,[a] Virginia Losasso,[b] Artur Ciesielski,[a] Paolo Samorì[a] and Massimo Bonini*[b]*

[a] University of Strasbourg & CNRS, ISIS & icFRC, 8 allee Gaspard Monge, 67000 Strasbourg, France
* Email: samori@unistra.fr

[b] Department of Chemistry "Ugo Schiff" and CSGI, University of Florence, via della Lastruccia 3, Sesto Fiorentino, Florence, 50019 Italy
* Email: massimo.bonini@unifi.it

Keywords: caseinate hydrogels, ionic crosslinking, protein hydrogels, soft electronics, flexible sensors

Table of Contents

S1. Experimental Section

S1.1 Materials

All the following products were purchased from Sigma Aldrich, without further purification: sodium caseinate (NaCas, 9005-46-3, 1.28% (w/w) of sodium ions contained), calcium chloride anhydrous ($CaCl_2$, 10043-52-4, ≥ 99.9%), strontium chloride hexahydrate ($SrCl_2 \cdot 6H_2O$, 10025-70-4, 99.0-103.0%), barium chloride anhydrous ($BaCl_2$, 10361-37-2, 99.9%), manganese chloride tetrahydrate ($MnCl_2 \cdot 4H_2O$, 221279, ≥ 98%), zinc chloride anhydrous ($ZnCl_2$, 7646-85-7, ≥ 98%), iron chloride anhydrous ($FeCl_3$, 7705-08-0, ≥ 99.9%), aluminum chloride anhydrous ($AlCl_3$, 7446-70-0, 99.9%), zirconium chloride anhydrous ($ZrCl_4$, 10026-11-6, 99.9%). Deionized water was used for all solution preparations. All reagents were used without further purification.

S1.2 MCas hydrogels preparation

Sodium caseinate hydrogels crosslinked with multivalent cations (MCas) were prepared by casting 5.0 g of a 20 % (w/v) NaCas aqueous solution into silicone molds. A cellulose paper sheet (pre-soaked in the crosslinking solution), onto which 10 mL of 0.5 M MCl_X solution ($M^{X+} = Ca^{2+}$, Sr^{2+}, Ba^{2+}, Mn^{2+}, Cu^{2+}, Zn^{2+}, Fe^{3+}, Al^{3+}, or Zr^{4+}), was placed as a front barrier to control the diffusion of the crosslinking ions into the protein matrix. The samples were allowed to crosslink for 4 h, followed by a 4 h washing step in 10 mL of deionized water. Each hydrogel was denoted MCas, where M corresponds to the crosslinking cation. The measured pH values were: Ca (8.77), Sr (3.87), Ba (5.90), Mn (5.69), Cu (3.64), Zn (5.56), Fe (~0), Al (2.81), Zr (~0). Volumetric shrinkage upon ionic crosslinking was evaluated by determining the gel volume before and after crosslinker addition: the initial volume was obtained from the NaCas solution's mass and density, while the final volume was measured by water displacement in a graduated cylinder and analyzed with *ImageJ* software.

S1.3 MGelCas organohydrogels preparation

MGelCas organohydrogels were prepared by dispersing 6.0 g of a 20 % (w/v) NaCas aqueous solution together with 4.0 g of gelatin Type A in 20 mL of deionized water under continuous stirring at 50 °C until complete dissolution. The homogeneous biopolymer mixture was then cast into PMMA molds (9.5 cm × 3.0 cm) and allowed to equilibrate at room temperature. Ionic crosslinking was achieved by immersing the cast samples in 0.5 M MCl_2 solutions ($M^{2+} = Sr^{2+}$, Zn^{2+}) prepared in a glycerol:water 1:2 (w/v) medium. The samples were maintained in the crosslinking bath for 1.5 h, enabling diffusion of the metal cations into the gel matrix.

Subsequently, the organohydrogels were transferred to a washing bath consisting of glycerol:water 1:2 (w/v) for an additional 1.5 h to remove excess ions while retaining the organophilic environment. The resulting hydrogels were dried overnight at ambient conditions to obtain freestanding organohydrogel strips. The typical thicknesses of the samples were ~930 μm for SrGelCas and ~630 μm for ZnGelCas (measured with a Mitutoyo digimatic micrometer).

S1.4 Characterization techniques

S1.4.1 Inductively coupled plasma-atomic emission spectrometry (ICP-AES)

The content of Na^{+}, Ca^{2+}, Sr^{2+}, Ba^{2+}, Mn^{2+}, Cu^{2+}, Zn^{2+}, Fe^{3+}, Al^{3+}, and Zr^{4+} in the MCas samples was quantified using an Agilent 720-ES ICP-AES instrument equipped with a pneumatic nebulizer. Approximately 10 mg of each sample was dissolved in 2 mL of 0.05 M Na_2EDTA and 10% (w/v) NaOH solution at 80 °C for 1 hour with magnetic stirring. After dilution, measurements were performed in triplicate using calibration lines from certified standards.

S1.4.2 Fourier-transform infrared spectroscopy (FTIR)

FTIR spectra of the dried MCas samples were acquired in ATR (Attenuated Total Reflectance) mode with a Thermo Nicolet Nexus 870 FT-IR spectrophotometer (Thermo Fisher Scientific, Waltham, MA, United States) equipped with a Golden Gate accessory. All the spectra were recorded with a resolution of 2 cm^{-1}, averaging 128 scans for measurement, in the range 4000–650 cm^{-1}.

S1.4.3 X-ray photoelectron spectroscopy (XPS)

X-ray Photoelectron Spectroscopy was performed on air-dried MCas samples by a Thermo Scientific K-Alpha X-ray photoelectron spectrometer, equipped with an aluminum X-ray source (energy 1.4866 keV) at a vacuum level of 10^{-8}-10^{-9} mbar in the main chamber. The spot size of the X-ray beam was fixed at 400 μm.

S1.4.4 Differential scanning calorimetry (DSC)

DSC measurements were performed using a Discovery DSC 2500 instrument. Air-dried samples, equilibrated at 40% RH were heated from 5 °C to 110 °C with a rate of 10 °C/min. Tzero Aluminum Hermetic pans (TA Instruments) were used for all the measurements. Data were processed with Trios v5.1.1.46572 software (TA Instruments).

S1.4.5 Small-angle X-ray scattering (SAXS)

Small-angle scattering measurements were performed using a Xeuss 3HR system with a scatterless collimation camera and a hybrid detector (Eiger 1M, Dectris). Cu Kα radiation (λ = 1.542 Å) was

produced by an ultra-brilliant point microfocus X-ray source (GENIX-Fox 3D, Xenocs, Grenoble) operating at 30 W. Measurements were taken at two sample-to-detector distances (400 mm and 1800 mm) to cover a q-range of 0.005 $Å^{-1}$ to 0.5 $Å^{-1}$. Data analysis was conducted using SasView software. (http://www.sasview.org/).

S1.4.6 Field Emission-Scanning Electron Microscopy (FE-SEM)

A Zeiss ΣIGMA FE-SEM (Oberkochen, Germany) was used to carry out the measurements. Samples prepared as described in Section S1.2 were freeze-dried when in the wet state, immediately after the washing step. The micrographs were acquired with an accelerating voltage of 2 kV, sample-detector distance 2-4 mm, aperture 10 μm and using the In-Lens detector.

S1.4.7 Compressive tests

Compressive properties MCas hydrogels (1.3 cm of diameter) were measured using a Discovery DHR-3 rheometer, using a head plate with 2 cm diameter. The compression speed was 20 μm/s.

S1.4.8 Electrical conductivity determination

MCas-based hydrogel disks (1.3 cm of diameter) were placed between two gold plates (2 x 2 cm) and then connected to a probe workstation (Keithley 2636B) to measure current variations. The related I-t curves were recorded applying a direct voltage of 0.2 V.

S1.4.9 MGelCas mechanical characterization: Tensile mechanical properties were evaluated using a Mark-10 M7-025E digital force gauge mounted on a Mark-10 ESM-303E motorized test stand. Gel strips were clamped at the edges, with a stretchable region of 2.5 cm.

S1.4.10 MGelCas Strain Sensitivity Measurements: Strain-sensing performance was measured using the same Mark-10 tensile setup. Gel samples (2.5 cm gauge length) were connected to the Keithley 2636B system, and current changes were recorded as I-t curves under an applied 0.5 V bias. For cycling stability measurements, the gauge length was reduced to 1 cm.

S2. MCas general properties

Table S1. Shrinking ratio (determined following the procedure in section S1.2) and M^{X+} content (determined through ICP-AES) for the MCas hydrogels.

Sample	Shrinking ratio	M^{X+} content (mmol/g of caseinate)
CaCas	0.98	0.79
SrCas	1.05	0.86
BaCas	0.98	0.95
MnCas	1.01	0.52
CuCas	0.93	1.48
ZnCas	0.66	0.80
FeCas	0.97	0.49
AlCas	0.56	0.38
ZrCas	1.03	0.65

S3. FTIR analysis

Table S2. Peak assignment of the spectra reported in **Figure 1b**. The error associated with the values is ± 2 cm^{-1}

Sample	δ (NH-CO) O.O.P. [cm^{-1}]	δ (NH-CO) I.P. [cm^{-1}]	ν(COO-) sym [cm^{-1}]	δ(N-H)/ν(C-N) amide I [cm^{-1}]	ν(COO-) asym [cm^{-1}]	ν(C=O) amide I [cm^{-1}]	ν(NH) amide I and II [cm^{-1}]
NaCas	975	1082	1398	1448	1538	1640	3291
CaCas	994	1092	1419	1447	1539	1635	3278
SrCas	988	1101	1419	1446	1540	1635	3281
BaCas	980	1096	1406	1446	1538	1635	3284
MnCas	996	1084	1419	1447	1539	1635	3283
CuCas	998	1081	/	1447	1517	1635	3283
ZnCas	1033	1082	/	1446	1529	1633	3252
FeCas	1014	1082	/	1445	1529	1634	3281
AlCas	1032	1107	/	1453	1530	1633	3275
ZrCas	878	1007	1407	1449	1535	1630	3283

S4. XPS analysis

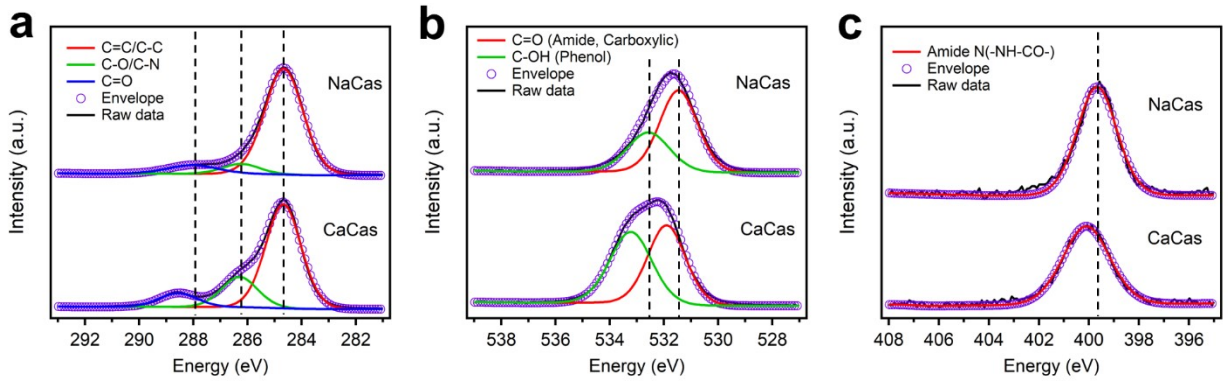

Figure S1. High-resolution XPS spectra of NaCas and CaCas gels: (a) C 1s, (b) O 1s, and (c) N 1s. The centers of the deconvolution bands are the following. **C 1s NaCas:** 284.68 eV (C=C/C-C); 286.28 eV (C-O/C-N); 288.08 eV (C=O). **C 1s CaCas:** 284.68 eV (C=C/C-C); 286.28 eV (C-O/C-N); 288.58 eV (C=O). **O 1s NaCas:** 531.48 eV (C=O, Amide, Carboxylic); 532.58 eV (C-OH, Phenol). **O 1s CaCas:** 531.88 eV (C=O, Amide, Carboxylic); 533.18 eV (C-OH, Phenol). **N 1s NaCas:** 399.68 eV (Amide N(-NH-CO-)). **N 1s CaCas:** 400.08 eV (Amide N(-NH-CO-)). Spectra are normalized with respect to the most intense peak.

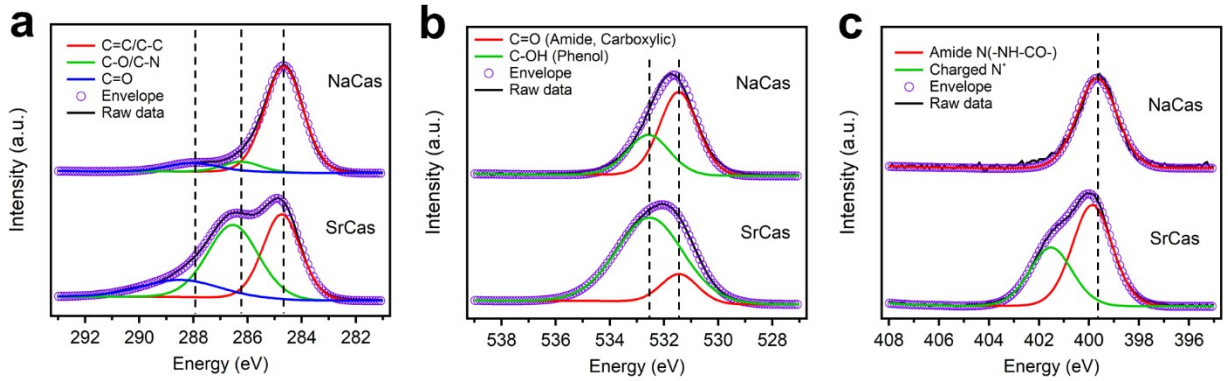

Figure S2. High-resolution XPS spectra of NaCas and SrCas gels: (a) C 1s, (b) O 1s, and (c) N 1s. The centers of the deconvolution bands are the following. **C 1s NaCas:** 284.68 eV (C=C/C-C); 286.28 eV (C-O/C-N); 288.08 eV (C=O). **C 1s SrCas:** 284.68 eV (C=C/C-C); 286.58 eV (C-O/C-N); 288.48 eV (C=O). **O 1s NaCas:** 531.48 eV (C=O, Amide, Carboxylic); 532.58 eV (C-OH, Phenol). **O 1s SrCas:** 531.38 eV (C=O, Amide, Carboxylic); 532.58 eV (C-OH, Phenol). **N 1s NaCas:** 399.68 eV (Amide N(-NH-CO-)). **N 1s SrCas:** 400.08 eV (Amide N(-NH-CO-)); 401.48 eV (Charged N^+). Spectra are normalized with respect to the most intense peak.

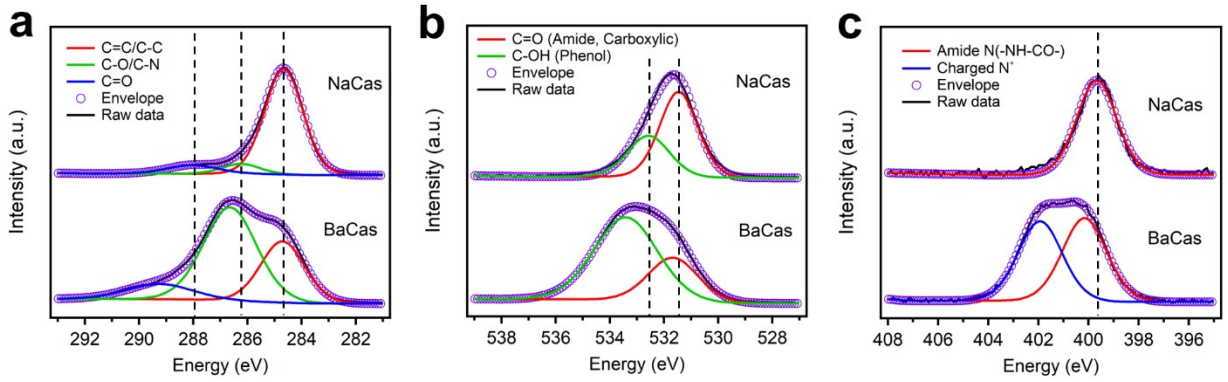

Figure S3. High-resolution XPS spectra of NaCas and BaCas gels: (a) C 1s, (b) O 1s, and (c) N 1s. The centers of the deconvolution bands are the following. **C 1s NaCas:** 284.68 eV (C=C/C-C); 286.28 eV (C-O/C-N); 288.08 eV (C=O). **C 1s BaCas:** 284.68 eV (C=C/C-C); 286.68 eV (C-O/C-N); 289.28 eV (C=O). **O 1s NaCas:** 531.48 eV (C=O, Amide, Carboxylic); 532.58 eV (C-OH, Phenol). **O 1s BaCas:** 531.68 eV (C=O, Amide, Carboxylic); 533.38 eV (C-OH, Phenol). **N 1s NaCas:** 399.68 eV (Amide N(-NH-CO-)). **N 1s BaCas:** 400.18 eV (Amide N(-NH-CO-)); 401.88 eV (Charged N^+). Spectra are normalized with respect to the most intense peak.

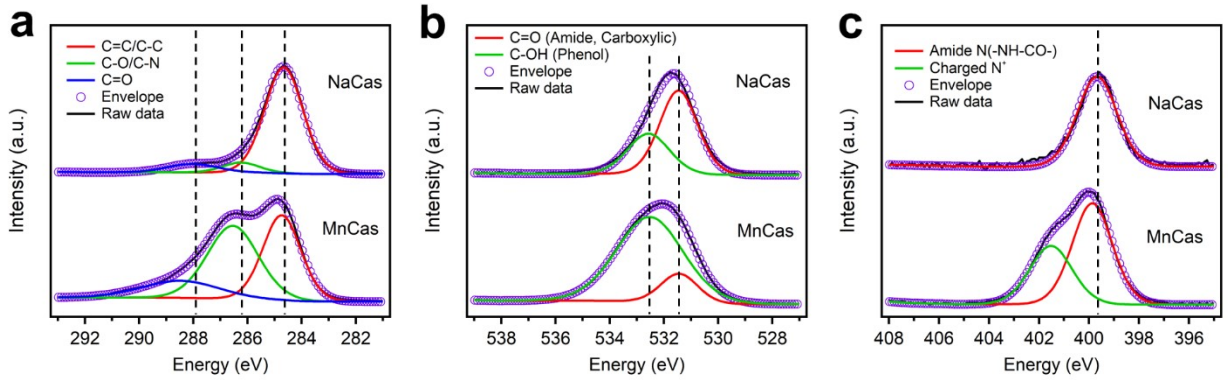

Figure S4. High-resolution XPS spectra of NaCas and MnCas gels: (a) C 1s, (b) O 1s, and (c) N 1s. The centers of the deconvolution bands are the following. **C 1s NaCas:** 284.68 eV (C=C/C-C); 286.28 eV (C-O/C-N); 288.08 eV (C=O). **C 1s MnCas:** 284.68 eV (C=C/C-C); 286.58 eV (C-O/C-N); 288.48 eV (C=O). **O 1s NaCas:** 531.48 eV (C=O, Amide, Carboxylic); 532.58 eV (C-OH, Phenol). **O 1s MnCas:** 531.38 eV (C=O, Amide, Carboxylic); 532.58 eV (C-OH, Phenol). **N 1s NaCas:** 399.68 eV (Amide N(-NH-CO-)). **N 1s MnCas:** 399.88 eV (Amide N(-NH-CO-)); 401.48 eV (Charged N^+). Spectra are normalized with respect to the most intense peak.

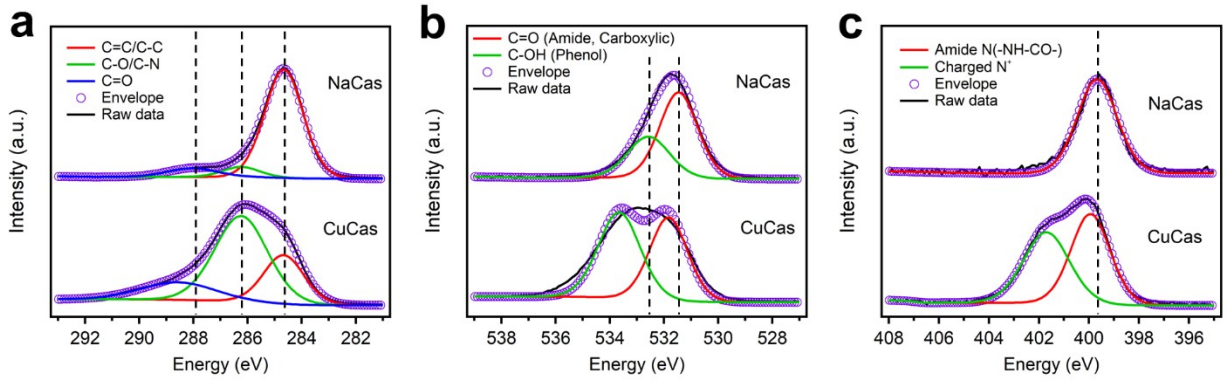

Figure S5. High-resolution XPS spectra of NaCas and CuCas gels: (a) C 1s, (b) O 1s, and (c) N 1s. The centers of the deconvolution bands are the following. **C 1s NaCas:** 284.68 eV (C=C/C-C); 286.28 eV (C-O/C-N); 288.08 eV (C=O). **C 1s CuCas:** 284.68 eV (C=C/C-C); 286.28 eV (C-O/C-N); 288.58 eV (C=O). **O 1s NaCas:** 531.48 eV (C=O, Amide, Carboxylic); 532.58 eV (C-OH, Phenol). **O 1s CuCas:** 531.78 eV (C=O, Amide, Carboxylic); 533.68 eV (C-OH, Phenol). **N 1s NaCas:** 399.68 eV (Amide N(-NH-CO-)). **N 1s CuCas:** 399.88 eV (Amide N(-NH-CO-)); 401.68 eV (Charged N^+). Spectra are normalized with respect to the most intense peak.

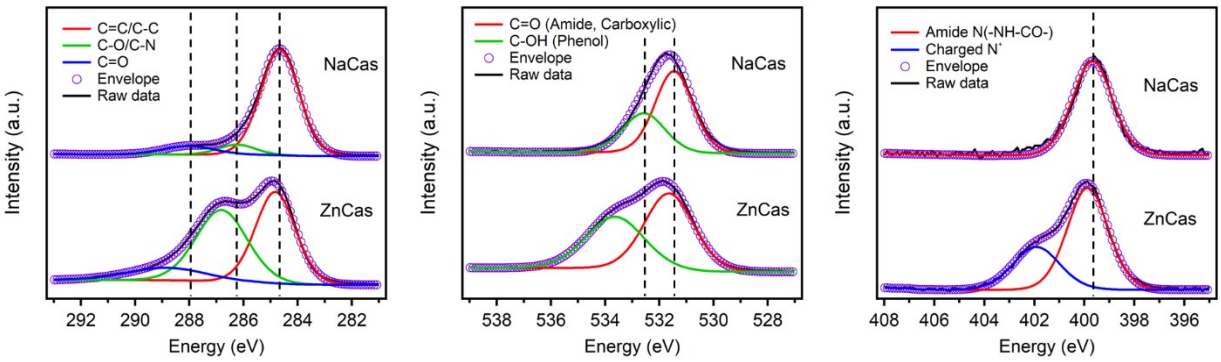

Figure S6. High-resolution XPS spectra of NaCas and ZnCas gels: (a) C 1s, (b) O 1s, and (c) N 1s. The centers of the deconvolution bands are the following. **C 1s NaCas:** 284.68 eV (C=C/C-C); 286.28 eV (C-O/C-N); 288.08 eV (C=O). **C 1s ZnCas:** 284.78 eV (C=C/C-C); 286.78 eV (C-O/C-N); 288.88 eV (C=O). **O 1s NaCas:** 531.48 eV (C=O, Amide, Carboxylic); 532.58 eV (C-OH, Phenol). **O 1s ZnCas:** 531.58 eV (C=O, Amide, Carboxylic); 533.58 eV (C-OH, Phenol). **N 1s NaCas:** 399.68 eV (Amide N(-NH-CO-)). **N 1s ZnCas:** 399.88 eV (Amide N(-NH-CO-)); 401.88 eV (Charged N^+). Spectra are normalized with respect to the most intense peak.

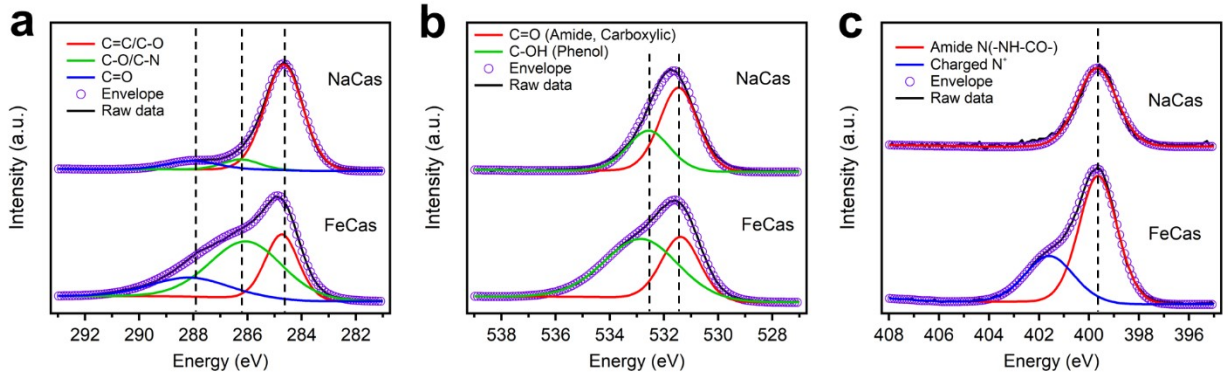

Figure S7. High-resolution XPS spectra of NaCas and FeCas gels: (a) C 1s, (b) O 1s, and (c) N 1s . The centers of the deconvolution bands are the following. **C 1s NaCas:** 284.68 eV (C=C/C-C); 286.28 eV (C-O/C-N); 288.08 eV (C=O). **C 1s FeCas:** 284.68 eV (C=C/C-C); 286.08 eV (C-O/C-N); 288.18 eV (C=O). **O 1s NaCas:** 531.48 eV (C=O, Amide, Carboxylic); 532.58 eV (C-OH, Phenol). **O 1s FeCas:** 531.38 eV (C=O, Amide, Carboxylic); 532.88 eV (C-OH, Phenol). **N 1s NaCas:** 399.68 eV (Amide N(-NH-CO-)). **N 1s FeCas:** 399.58 eV (Amide N(-NH-CO-)); 401.58 eV (Charged N^+). Spectra are normalized with respect to the most intense peak.

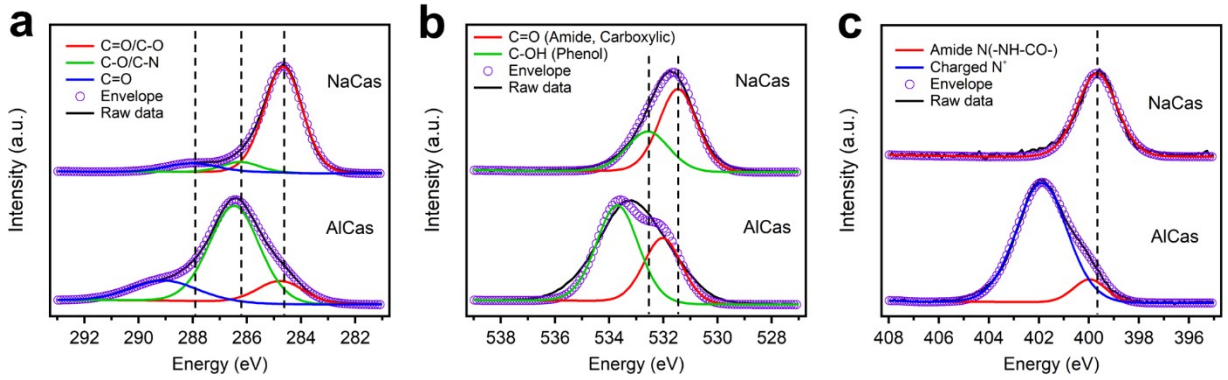

Figure S8. High-resolution XPS spectra of NaCas and AlCas gels: (a) C 1s, (b) O 1s, and (c) N 1s. The centers of the deconvolution bands are the following. **C 1s NaCas:** 284.68 eV (C=C/C-C); 286.28 eV (C-O/C-N); 288.08 eV (C=O). **C 1s AlCas:** 284.68 eV (C=C/C-C); 286.48 eV (C-O/C-N); 289.08 eV (C=O). **O 1s NaCas:** 531.48 eV (C=O, Amide, Carboxylic); 532.58 eV (C-OH, Phenol). **O 1s AlCas:** 531.98 eV (C=O, Amide, Carboxylic); 533.68 eV (C-OH, Phenol). **N 1s NaCas:** 399.68 eV (Amide N(-NH-CO-)). **N 1s AlCas:** 399.98 eV (Amide N(-NH-CO-)); 401.88 eV (Charged N^+). Spectra are normalized with respect to the most intense peak.

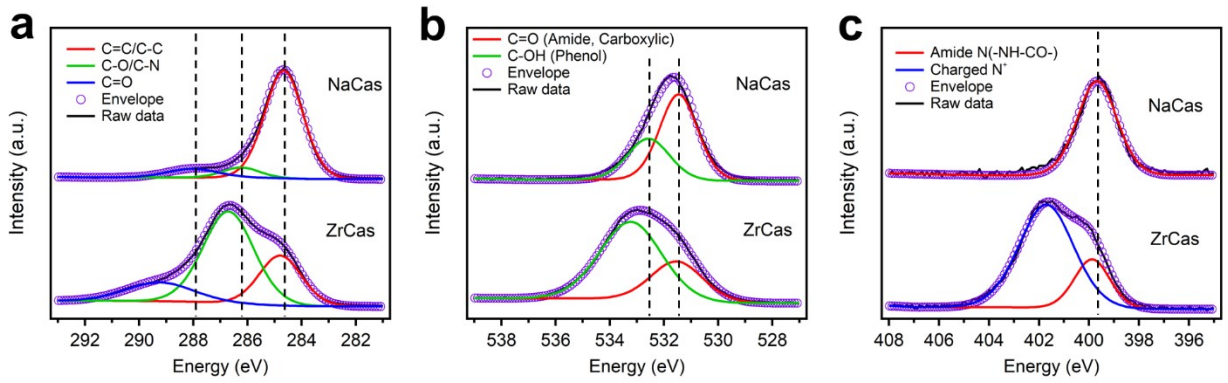

Figure S9. High-resolution XPS spectra of NaCas and ZrCas gels: (a) C 1s, (b) O 1s, and (c) N 1s. The centers of the deconvolution bands are the following. **C 1s NaCas:** 284.68 eV (C=C/C-C); 286.28 eV (C-O/C-N); 288.08 eV (C=O). **C 1s ZrCas:** 284.78 eV (C=C/C-C); 286.68 eV (C-O/C-N); 289.18 eV (C=O). **O 1s NaCas:** 531.48 eV (C=O, Amide, Carboxylic); 533.18 eV (C-OH, Phenol). **O 1s ZrCas:** 531.48 eV (C=O, Amide, Carboxylic); 533.68 eV (C-OH, Phenol). **N 1s NaCas:** 399.68 eV (Amide N(-NH-CO-)). **N 1s ZrCas:** 399.88 eV (Amide N(-NH-CO-)); 401.68 eV (Charged N^+). Spectra are normalized with respect to the most intense peak.

S5. DSC analysis

Table S3. Glass transition temperatures (T_g) of the MCas sample, extracted from the thermograms in Figure 2a. The error associated with the given values is ± 1.0 °C

NaCas	CaCas	SrCas	BaCas	MnCas	CuCas	ZnCas	FeCas	AlCas	ZrCas
72.2 °C	73.3 °C	71.7 °C	72.2 °C	75.1 °C	74.6 °C	75.0 °C	74.3 °C	76.6 °C	75.6 °C

S6. SAXS analysis

The SAXS curves displayed in **Figure 2b** were fitted within the q-range of 0.02 – 0.5 $Å^{-1}$. For the ZrCas sample, the fitting range was extended down to 0.01 $Å^{-1}$ to improve the quality of the fit, as the slope exhibits a marked change around 0.02 $Å^{-1}$, potentially affecting the accuracy of the fitting. For the NaCas curve, the following equation was employed to fit the peak associated with the presence of micelles within the viscous polymeric solution:

$$I(q) = \frac{A}{\left(1 + \left(\frac{q - q_0}{B}\right)^2\right)} + bkg \qquad \text{Eq. S1}$$

where A is a scale factor, B represents the half-width at half-maximum of the peak, and bkg is the background signal. The peak observed at q = 0.031 $Å^{-1}$ indicates that the micelles are ~ 20.3 nm apart.

In contrast, the presence of crosslinking significantly alters the micellar assembly, leading to smoother SAXS curves. Therefore all the other MCas curves were best fitted using the following model [1-6]:

$$I(q) = \frac{A}{q^k} + \frac{B}{1 + (q\xi_1)^m} + \frac{C}{1 + (q\xi_2)^n} + bkg \qquad \text{Eq. S2}$$

where bkg is the background signal, A is the Porod scale factor, and k is the corresponding Porod exponent. B and C are Lorentzian scale factors, while ξ_1 and ξ_2 denote the respective correlation lengths. The parameters m and n correspond to the associated power-law exponents. The extracted long-distance (ξ_1) and short-distance (ξ_2) correlation lengths are summarized in **Table S4**, along with the other fitting parameters. For consistency, the primary correlation length, ξ_1—associated with the low-q Lorentzian term and obtainable for every sample—is used for all cross-sample comparisons in the main text, as it reflects the dominant average spacing between crosslinked domains.

For consistency, ξ_1—associated with the low-q Lorentzian term and obtainable for all samples—is used for cross-sample comparisons in the main text, as it reflects the dominant average spacing between crosslinked domains. Notably, variations in ξ_1 report on ion-dependent nanoscale density fluctuations within the hydrated network, whereas the similar morphologies observed by SEM arise from the mesoscale topology of the dried skeleton and therefore do not mirror these local structural differences [7-8].

Table S4. SAXS fitting parameters (Eq. S2) for the MCas curves illustrated in **Figure 2b**.

	CaCas	**SrCas**	**BaCas**	**MnCas**	**CuCas**	**ZnCas**	**FeCas**	**AlCas**	**ZrCas**
bkg	0.038	0.031	0.049	0.063	0.034	0.032	0.072	0.060	0.081
A	-	-	-	-	-	$8.1 \cdot 10^{-5}$	-	-	$9.8 \cdot 10^{-6}$
k	-	-	-	-	-	3.24	-	-	3.50
B	20.5	35.7	31.5	20.7	10.17	0.47	8.43	12.4	4.43
C	0.56	0.39	0.56	0.74	0.10	-	-	-	-
ξ_1 ***(nm)***	4.7±0.2	5.4±0.3	6.4±0.3	5.1±0.3	2.9±0.2	1.0±0.1	2.6±0.1	2.6±0.1	2.3±0.1
ξ_2 ***(nm)***	1.0±0.1	0.9±0.1	0.8±0.1	1.0±0.1	0.4±0.1	-	-	-	-
m	3.94	3.89	3.29	3.28	3.38	1.50	3.00	3.28	2.06
n	2.86	2.43	2.51	2.55	4.70	-	-	-	-

S7. Scanning electron microscopy (SEM)

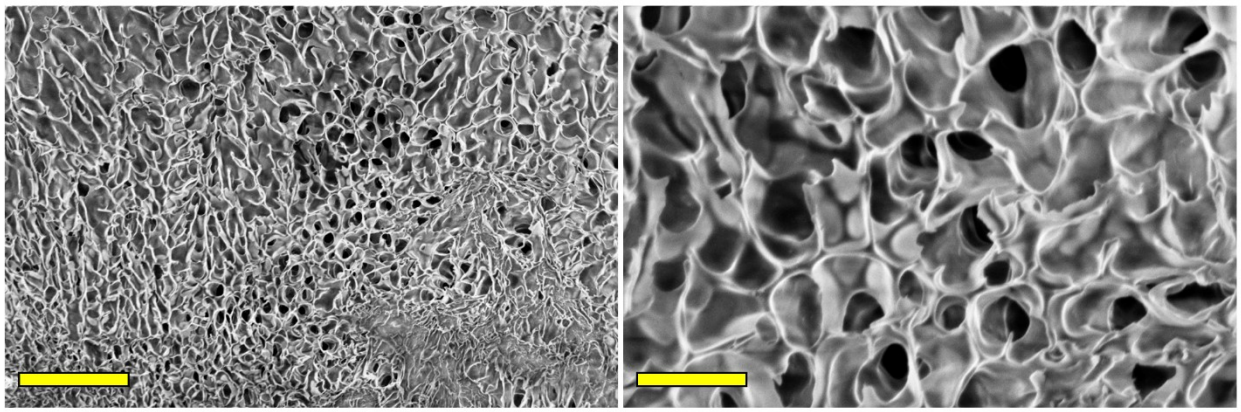

Figure S10. SEM micrographs of NaCas at different magnifications. The scale bars correspond to 8 µm (left panel) and 2 µm (right panel).

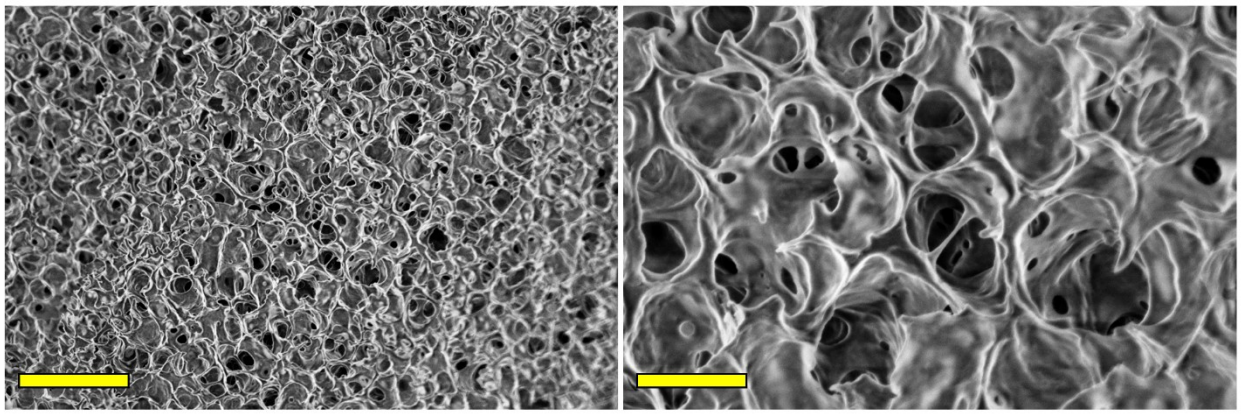

Figure S11. SEM micrographs of CaCas at different magnifications. The scale bars correspond to 8 µm (left panel) and 2 µm (right panel).

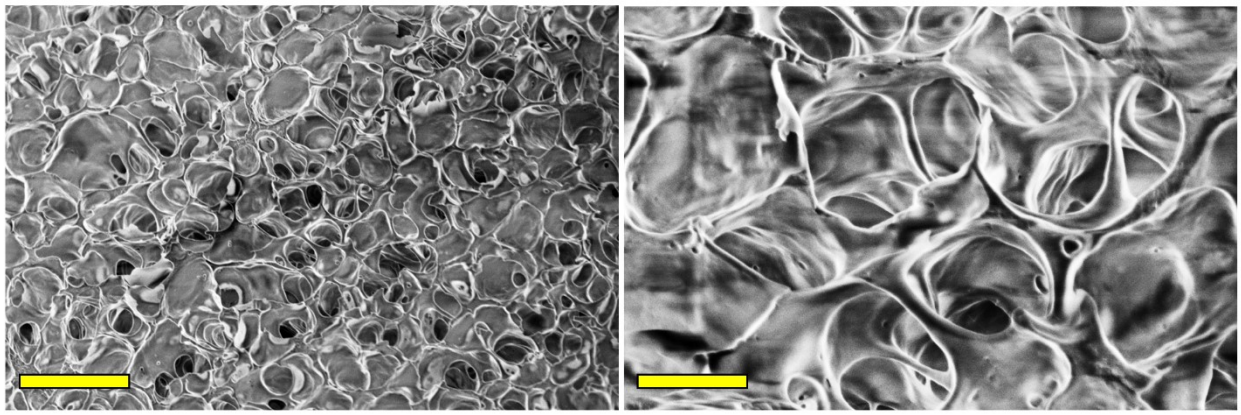

Figure S12. SEM micrographs of SrCas at different magnifications. The scale bars correspond to 8 µm (left panel) and 2 µm (right panel).

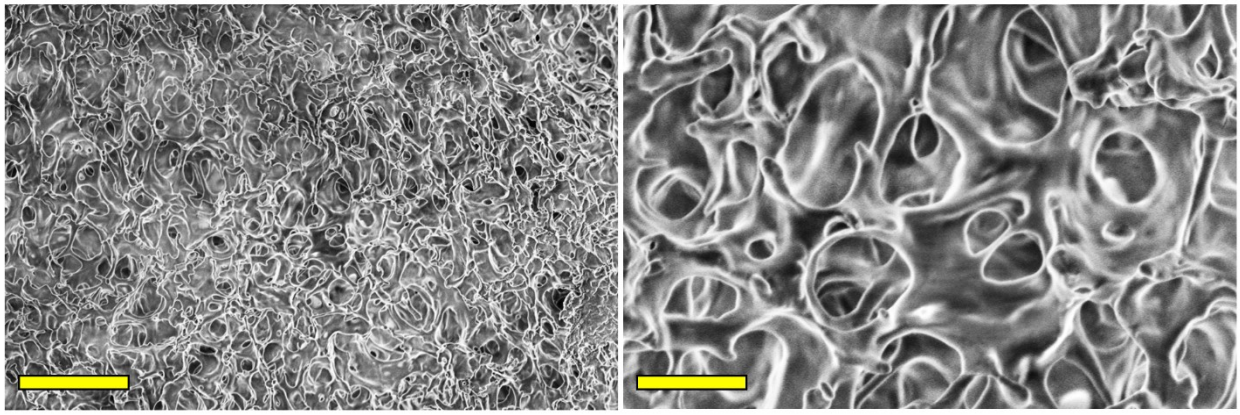

Figure S13. SEM micrographs of BaCas at different magnifications. The scale bars correspond to 8 µm (left panel) and 2 µm (right panel).

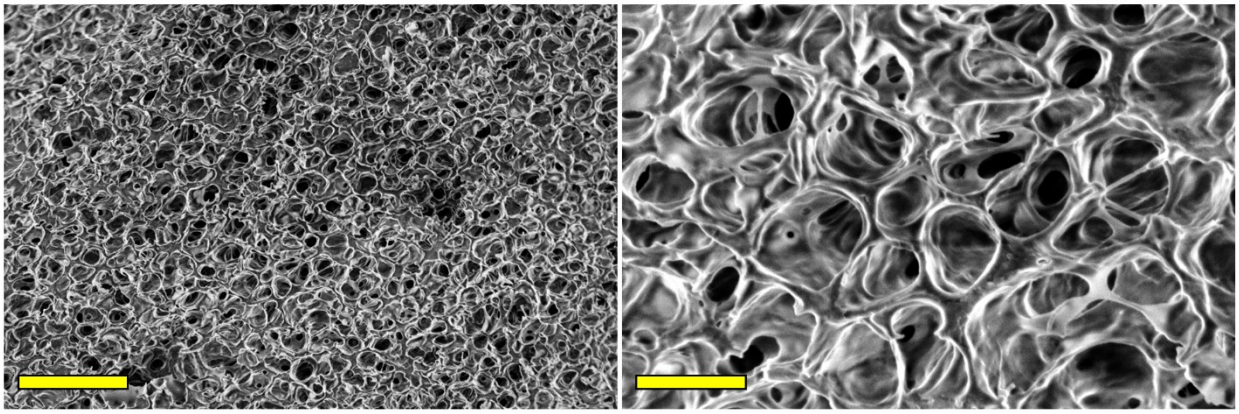

Figure S14. SEM micrographs of MnCas at different magnifications. The scale bars correspond to 8 µm (left panel) and 2 µm (right panel).

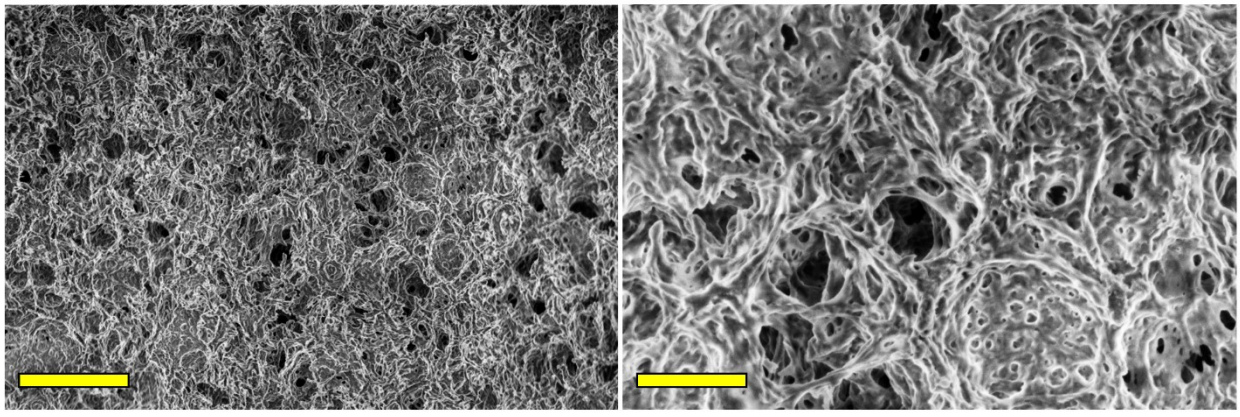

Figure S15. SEM micrographs of CuCas at different magnifications. The scale bars correspond to 8 µm (left panel) and 2 µm (right panel).

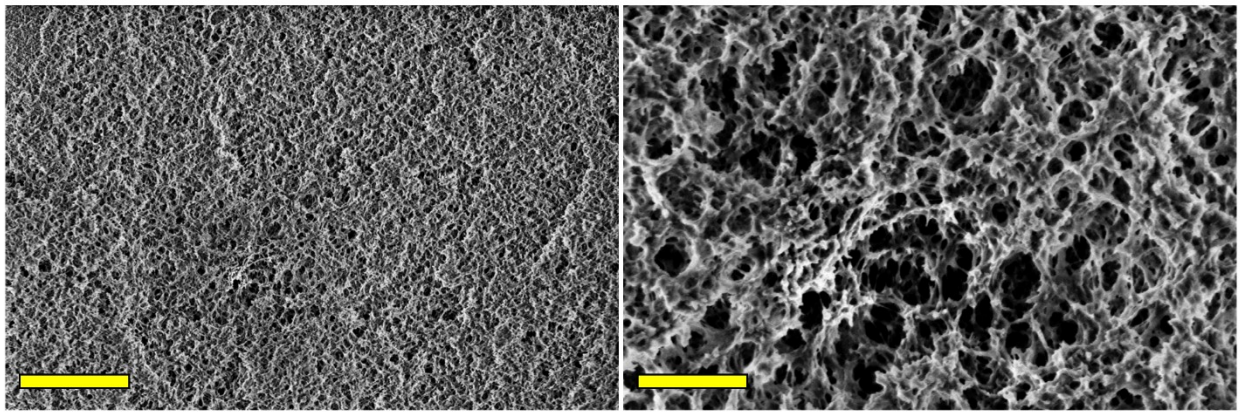

Figure S16. SEM micrographs of ZnCas at different magnifications. The scale bars correspond to 8 µm (left panel) and 2 µm (right panel).

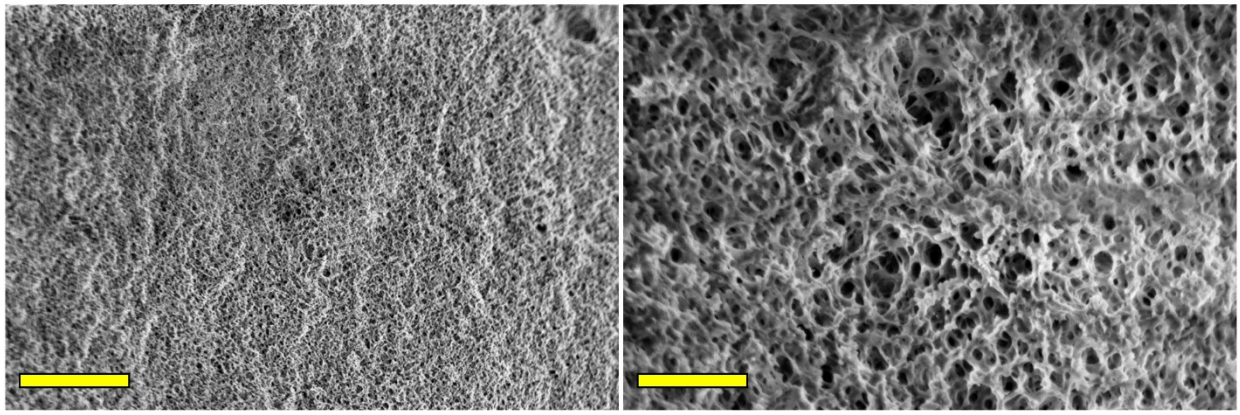

Figure S17. SEM micrographs of FeCas at different magnifications. The scale bars correspond to 8 µm (left panel) and 2 µm (right panel).

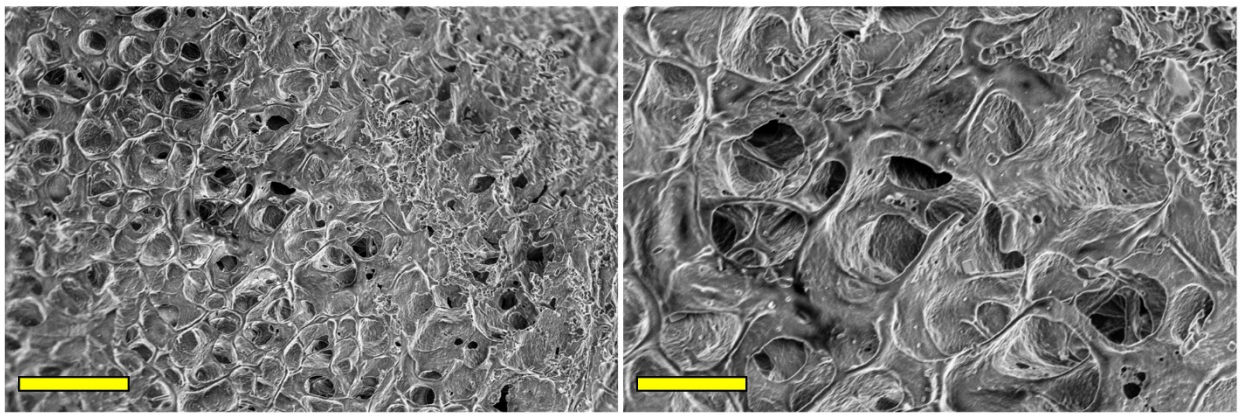

Figure S18. SEM micrographs of AlCas at different magnifications. The scale bars correspond to 20 µm (left panel) and 8 µm (right panel).

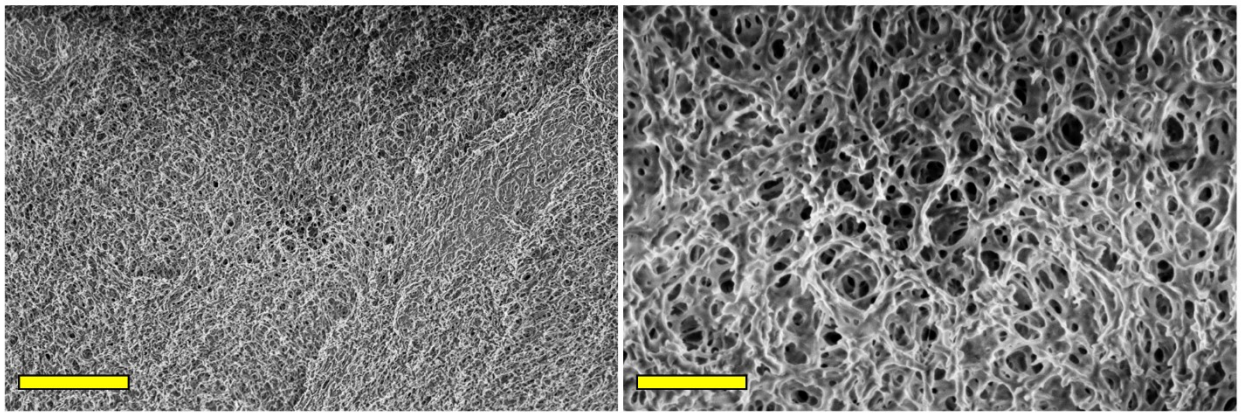

Figure S19. SEM micrographs of ZrCas at different magnifications. The scale bars correspond to 8 μm (left panel) and 2 μm (right panel).

S8. MCas response to compression

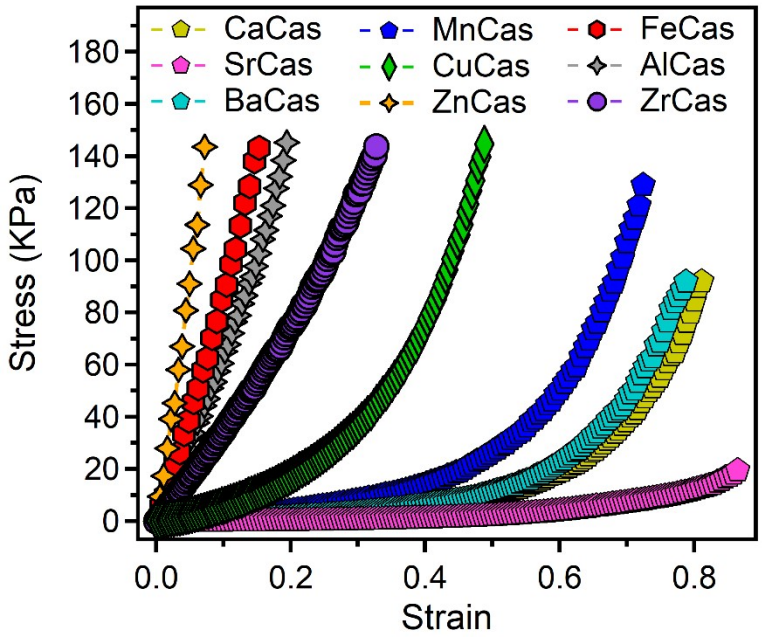

Figure S20. Full-range compressive stress-strain curves of the MCas samples, illustrating their mechanical response under compression.

Table S5. Compressive moduli of the MCas samples, extracted from the stress-strain curves in **Figure S20** over the 0.00–0.07 strain range.

Sample	**Compressive modulus (kPa)**
CaCas	8.3 ± 0.2
SrCas	1.6 ± 0.3
BaCas	8.2 ± 0.8
MnCas	11.4 ± 0.5
CuCas	75.9 ± 2.9
ZnCas	1792 ± 170
FeCas	844 ± 36
AlCas	557 ± 61
ZrCas	359 ± 34

S9. MCas conductivity evaluation

Table S6. Conductivity of the MCas samples.

Sample	Conductivity (mS/m)
CaCas	0.234 ± 0.012
SrCas	0.011 ± 0.001
BaCas	0.013 ± 0.001
MnCas	0.020 ± 0.001
CuCas	13.5 ± 0.7
ZnCas	0.023 ± 0.001
FeCas	5.91 ± 0.31
AlCas	0.095 ± 0.005
ZrCas	0.052 ± 0.003

S10. Optical, Mechanical, and Piezoresistive Properties of MGelCas

Figure S21. Photograph of SrGelCas (left) and ZnGelCas (right) organohydrogel strips demonstrating their high optical transparency.

Table S7. Thickness, Young's modulus (YM, evaluated in the 0.0-0.5 strain range), ultimate tensile strength (UTS), gauge factor (GF) and gauge factor normalized by the Young's modulus (GF/YM) of SrGelCas and ZnGelCas.

Sample	Thickness (μm)	YM (MPa)	UTS (MPa)	GF	GF/YM (MPa^{-1})
SrGelCas	931 ± 60	0.076 ± 0.013	0.18 ± 0.04	1.84 ± 0.11	~24.2
ZnGelCas	634 ± 22	0.232 ± 0.089	0.83 ± 0.07	2.20 ± 0.13	~9.5

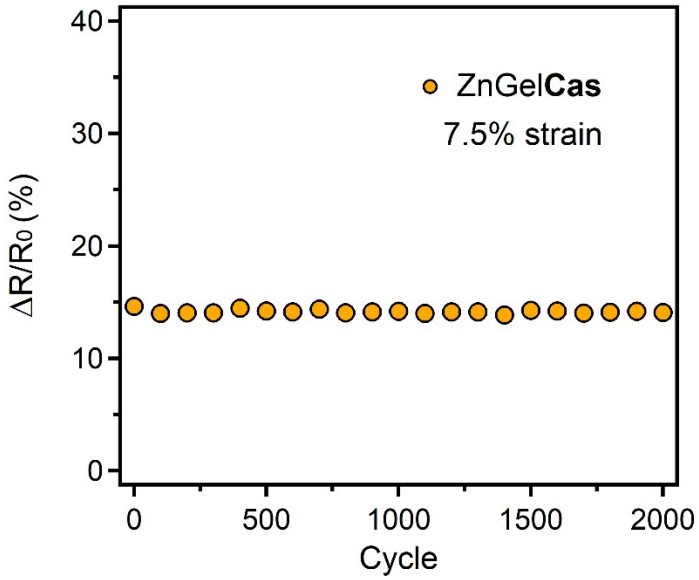

Figure S22. Long-term cyclic piezoresistive response of ZnGelCas under repeated tensile deformation at fixed strain (7.5%). The relative resistance variation ($\Delta R/R_0$) remains stable over 2000 deformation cycles, evidencing sustained signal reproducibility under prolonged operation. This behavior highlights the robustness of the Zn^{2+}-crosslinked network under demanding cyclic loading conditions.

S11. References

[1] Tordi, P.; Montes-García, V.; Tamayo, A.; Bonini, M.; Samorì, P.; Ciesielski, A. Ionically Tunable Gel Electrolytes Based on Gelatin-Alginate Biopolymers for High-Performance Supercapacitors. *Small* 2025, 2503937. https://doi.org/10.1002/smll.202503937.

[2] Tordi, P.; Gelli, R.; Tamantini, S.; Bonini, M. Alginate Crosslinking beyond Calcium: Unlocking the Potential of a Range of Divalent Cations for Fiber Formation. *Int. J. Biol. Macromol.* 2025, 306, 141196. https://doi.org/10.1016/j.ijbiomac.2025.141196.

[3] Hammouda, B.; Worcester, D. The Denaturation Transition of DNA in Mixed Solvents. *Biophys. J.* 2006, 91 (6), 2237–2242. https://doi.org/10.1529/biophysj.106.083691.

[4] Hule, R. A.; Nagarkar, R. P.; Altunbas, A.; Ramay, H. R.; Branco, M. C.; Schneider, J. P.; Pochan, D. J. Correlations between Structure, Material Properties and Bioproperties in Self-Assembled β-Hairpin Peptide Hydrogels. *Faraday Discuss.* 2008, 139 (0), 251–264. https://doi.org/10.1039/B717616C.

[5] Ochbaum, G.; Bitton, R. 14 - Using Small-Angle X-Ray Scattering (SAXS) to Study the Structure of Self-Assembling Biomaterials. In Self-assembling Biomaterials; Azevedo, H. S., da Silva, R. M. P., Eds.; Woodhead Publishing Series in Biomaterials; Woodhead Publishing, 2018; pp 291–304. https://doi.org/10.1016/B978-0-08-102015-9.00015-0.

[6] Saffer, E. M.; Lackey, M. A.; Griffin, D. M.; Kishore, S.; Tew, G. N.; Bhatia, S. R. SANS Study of Highly Resilient Poly(Ethylene Glycol) Hydrogels. *Soft Matter* 2014, 10 (12), 1905–1916. https://doi.org/10.1039/C3SM52395K.

[7] Katrantzi, D.; Micklethwaite, S.; Hondow, N.; Brown, A.; Dougan, L. Unveiling the Structure of Protein-Based Hydrogels by Overcoming Cryo-SEM Sample Preparation Challenges. *Faraday Discuss.* **2025**, *260* (0), 55–81. https://doi.org/10.1039/D4FD00204K

[8] McDowall, D.; J. Adams, D.; M. Seddon, A. Using Small Angle Scattering to Understand Low Molecular Weight Gels. *Soft Matter* **2022**, *18* (8), 1577–1590. https://doi.org/10.1039/D1SM01707A